Three-dimensional aspects of matrix assembly by cells in the developing cornea

Robert D. Young[a,1], Carlo Knupp[a,1], Christian Pinali[a], Kenneth M.Y. Png[b], James R. Ralphs[c], Andrew J. Bushby[b], Tobias Starborg[d], Karl E. Kadler[d], and Andrew J. Quantock[a,2]

[a]Structural Biophysics Group, Cardiff Centre for Vision Science, School of Optometry and Vision Sciences, Cardiff University, Cardiff CF24 4HQ, Wales, United Kingdom; [b]The NanoVision Centre, School of Engineering and Materials Science, Queen Mary University of London, London E1 4NS, United Kingdom; [c]Connective Tissue Biology Laboratory, School of Biosciences, Cardiff University, Cardiff CF10 3AX, Wales, United Kingdom; and [d]Wellcome Trust Centre for Cell-Matrix Research, Faculty of Life Sciences, University of Manchester, Manchester M13 9PT, United Kingdom

Edited by David D. Sabatini, New York University School of Medicine, New York, NY, and approved November 8, 2013 (received for review July 23, 2013)

Cell-directed deposition of aligned collagen fibrils during corneal embryogenesis is poorly understood, despite the fact that it is the basis for the formation of a corneal stroma that must be transparent to visible light and biomechanically stable. Previous studies of the structural development of the specialized matrix in the cornea have been restricted to examinations of tissue sections by conventional light or electron microscopy. Here, we use volume scanning electron microscopy, with sequential removal of ultrathin surface tissue sections achieved either by ablation with a focused ion beam or by serial block face diamond knife microtomy, to examine the microanatomy of the cornea in three dimensions and in large tissue volumes. The results show that corneal keratocytes occupy a significantly greater tissue volume than was previously thought, and there is a clear orthogonality in cell and matrix organization, quantifiable by Fourier analysis. Three-dimensional reconstructions reveal actin-associated tubular cell protrusions, reminiscent of filopodia, but extending more than 30 μm into the extracellular space. The highly extended network of these membrane-bound structures mirrors the alignment of collagen bundles and emergent lamellae and, we propose, plays a fundamental role in dictating the orientation of collagen in the developing cornea.

Connective tissues fulfill diverse functions but conform to a general structural plan of cells surrounded by an extracellular matrix in which collagen is the main structural element (1, 2). Composition and tissue-specific organization of the component collagen fibrils are considered to be critically important for the functional properties of any particular tissue. The unique transparent quality of the cornea arises from its remarkably ordered architecture of aligned and regularly spaced fibrils with a small, consistent diameter (~30 nm), which are arranged, not into fibers or fascicles as in most other tissues but in superimposed, flattened layers, or lamellae. Lamellae and their component collagen fibrils exhibit preferential orientations throughout the corneal thickness (3), which appear to be closely related to the biomechanical loads to which the tissue is subjected. In adult vertebrates, lamellae traverse the full diameter of the cornea for most of its thickness, and in the avian eye—the subject of most developmental studies—undergo a gradual rotation in their orientation with depth (4). Individual collagen fibrils within midstromal lamellae also appear to traverse the entire diameter of the cornea, a distance of ~11 mm in adult human eyes. The extraordinary level of order in matrix organization within a hierarchy of fibril, lamella, and stroma overall appears to reflect a considerable level of regulatory influence presumably involving both cell activity and intermolecular interactions.

Collagen fibrils exhibit a microfibrillar substructure (5–7), undergoing self-assembly spontaneously in vitro from soluble monomeric collagen in a process largely dependent upon the physicochemical properties of collagen molecules, and which has been the subject of intensive study (8, 9). Type V collagen, a component of heterotypic type I/V fibrils in cornea (10), has been shown to contribute to the production of small-diameter fibrils, with its retained α1(V) *N*-propeptide domain implicated as modulator (11, 12). In vivo as well, evidence from studies of gene knockout mice suggests that type V collagen is a potent modulator of corneal fibril diameter (13, 14), although coordinated interaction between this and other factors potentially indicates a more complex regulatory control in the tissue microenvironment.

Mechanisms governing the deposition of tissue-specific, suprafibrillar architectures by cells in different tissues are even less well-understood than those controlling individual fibril formation. Developing tendon has been the most widely studied tissue in this regard (15–20). Collagen fibrils nucleate and form bundles within cell surface channels (15), or in intracellular inclusions, termed fibripositors (19), and sequentially undergo fusion (21) in the extracellular space to give rise to fascicles of uniaxial collagen. This process, occurring juxtaposed to the cell, would perhaps be expected to take place within a physicochemical environment influenced by the activity of the cell. An alternative mechanism, driven by intrinsic molecular interactions and potentially less dependent on direct cellular intervention, has also been proposed in which concentrated collagen solutions form organized liquid crystalline arrays that undergo spontaneous assembly into fibrils to generate specific tissue architectures (22–24). This process would be advantageous in allowing aligned collagen structures to form at relatively long distances from the cell (25), although evidence for its occurrence in vivo has not yet been obtained.

Significance

The cornea is a specialized connective tissue assembled as a remarkably ordered array of superimposed collagenous lamellae, and their component collagen fibrils, essential for optical transparency. Surprisingly, the mechanisms involved in deposition of this unique structure are still not fully understood. Here we have used correlative microscopy techniques, including innovative methods of serial block face scanning electron microscopy, to observe the sequence of corneal matrix formation in three-dimensional reconstructions of embryonic chick cornea. Our data show that corneal cells, keratocytes, exhibit long-range associations with collagen bundles in the developing matrix via an extended network of actin-rich tubular cytoplasmic protrusions, which we term *keratopodia*. Synchronized alignment of keratopodia and collagen is evident during the course of lamella formation.

Author contributions: A.J.Q. designed research; R.D.Y., C.K., K.M.Y.P., J.R.R., A.J.B., T.S., and K.E.K. performed research; R.D.Y., C.K., C.P., and A.J.Q. analyzed data; and R.D.Y., C.K., K.E.K., and A.J.Q. wrote the paper.

The authors declare no conflict of interest.

This article is a PNAS Direct Submission.

Freely available online through the PNAS open access option.

[1]R.D.Y. and C.K. contributed equally to this work.

[2]To whom correspondence should be addressed. E-mail: QuantockAJ@cf.ac.uk.

This article contains supporting information online at www.pnas.org/lookup/suppl/doi:10.1073/pnas.1313561110/-/DCSupplemental.

Observations on the establishment of mesoscopic tissue organization in the cornea have been few since the early classic studies by Hay et al. (26, 27) on the developing chick. These studies showed that epithelial cells secreted orthogonally disposed collagen fibrils as a rudimentary primary stroma, which was then invaded by mesenchymal cells—presumptive keratocytes, which deposited the secondary stroma of lamellae, characteristic of the mature tissue. An innovative study of chicken embryo cornea by Birk and Trelstad (28) using high-voltage electron microscopy on 0.5–1.0-μm–thick sections subsequently revealed more intricate detail of cellular morphology and collagen fibril and bundle accretion into lamellae.

Our understanding, in a 3D context, of the cellular mechanisms involved in fibrillogenesis and lamellogenesis, which underpin the formation of the corneal stroma, remains incomplete. Recent advances in technology have made it possible to gain 3D information at subcellular levels of resolution and in tissue volumes of many cubic microns (29–32). Collection of images of a specimen surface, alternating with surface renewal, enables many serial images to be acquired for 3D reconstruction. Focused ion beam scanning electron microscopy (FIB SEM) uses a Gallium ion beam to mill away the surface (30, 33). Alternatively, a slice can be removed from the specimen surface with an ultramicrotome within the microscope chamber (serial block face scanning electron microscopy, SBF SEM) (34, 35). Here, both of these approaches have been exploited to reveal unique features of corneal keratocytes, which appear crucial for both production of ordered collagen arrays and their assembly into lamellae in the developing corneal stroma.

Results

At 10 d of chicken embryonic development, early rudiments of corneal lamellae appeared as fibril bundles located within surface involutions of keratocytes and with extensions of their cell membranes (Fig. 1 *A* and *B*). Unidirectional alignment of fibrils with individual cells was observed, and some cells were associated with 2–5 bundles each with fibrils in different orientations (Fig. 1*A*). Fibril-free spaces represented a prominent feature of the stroma at this developmental stage. Development through 14 and 18 d was characterized by a more flattened cellular profile and a reduction in fibril-free extracellular spaces, owing to the continued deposition of aligned collagen (Fig. 1 *C*–*F*).

Reverse-contrast backscatter electron images from FIB SEM at days 10, 14, and 18 showed details of cells and organelles comparable to transmission electron microscopy (Fig. S1), except that at 6,000× magnification, used here, individual collagen fibrils could not be clearly resolved. Fly-through observation of the day 10 dataset (Movie S1) and 3D reconstructions (Fig. S2 *A* and *B* and Fig. S3 *A* and *B*; Movie S2 and Movie S3) confirmed that at this stage the developing stroma was characterized by a loose matrix, with abundant open spaces. Measurements based on threshold contrast differential between cell and matrix components indicated that each occupied ∼20% of the volume (Table 1).

Rounded cells exhibited a high level of membrane activity with numerous cell processes and projections, from small cylindrical finger-like extensions to flattened veils. All appeared closely apposed to collagen fibril bundles. Some cell involutions, enveloping collagen fibril bundles, ran for several microns into the sectioned volume. Cell- and collagen-free spaces were much reduced at day 14 (Fig. 1 *C* and *D*; Fig. S1*B*). A fly-through sequence of the dataset (Movie S4), and 3D reconstructions of cells and collagen

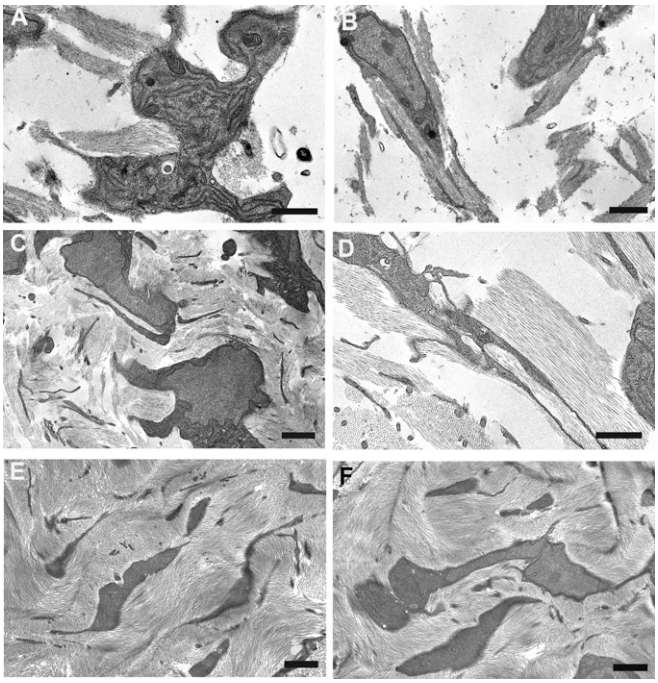

Fig. 1. Transmission electron microscopy from ultrathin sections of Durcupan-embedded chick corneal stroma at embryonic days 10 (*A* and *B*), 14 (*C* and *D*), and 18 (*E* and *F*). Keratocytes adopt flattened morphology with extended cell processes. Collagen bundles appear at cell surfaces in cell recesses and parallel to cell processes at days 10 and 14. Bundles form a lamellar structure at day 18. (Scale bars, 2 μm, 500 nm in *D*.)

(Fig. S2 *C* and *D* and Fig. S3 *C* and *D*; Movie S5 and Movie S6, respectively), revealed the flattened appearance of cells in the growing matrix. Collagen occupancy of the overall sample volume was increased over day 10 to ∼50%, with cells still representing 20% of the total volume (Table 1). The orthogonal arrangement of cells at this stage was striking, whereas membrane involutions associated with small fibril bundles appeared less evident. Collagen bundles were flattened, elongated, and, as at day 10, again associated with cytoplasmic processes from the cells. The extensive nature of cell processes was a conspicuous feature of the stroma at day 14 (Fig. S1*B* and Fig. S2*C*; Movie S5). Resembling filopodia, these were often relatively straight cylindrical structures—with a minimum diameter of ∼100 nm, extending in length beyond the full 30 μm width of the image field, or flattened in the plane of section, and occasionally branching. All appeared to be closely apposed to the surfaces of collagen bundles, although not always along their entire length. Immunofluorescence microscopy with AlexaFluor 488–conjugated phalloidin indicated strong staining for actin throughout the filopodia-like processes, which formed an orthogonal network (Fig. 2).

Intrastromal spaces were almost absent in the developing tissue at day 18 (Fig. 1 *E* and *F*; Fig. S1*C*, Fig. S2 *E* and *F*, and Fig. S3 *E* and *F*), when collagenous matrix constituted 70% of the sample volume and cells, 20% (Table 1). Cells and elongate processes defined the borders of lamellae, running an undulating course (Movie S7 and Movie S8). Filopodia-like processes persisted,

Table 1. Summary of cell and matrix volumes calculated from image series obtained from chick corneas at three embryonic stages by FIB SEM

Embryonic day	Sample volume, μm^3	Cell volume, %	Matrix volume, %	*z* depth, μm
10	1.2×10^4	18	20	23
14	0.6×10^4	20	50	11.5
18	1.5×10^4	20	70	28.5

but appeared shorter and less abundant than at day 14 (Movie S8). Collagen bundles were now coalesced into superimposed sheets, resembling the lamellae of mature tissue (Movie S7 and Movie S9). Collagen fibrils and filopodia-like processes ran parallel to each other along two orthogonal directions as early as day 12, which was verified quantitatively (Fig. 3) by the Fourier transform of the projections of 16 randomly selected volumes, each measuring $3.0 \times 3.0 \times 0.3$ μm^3. As expected from parallel filiform structures running along mutually orthogonal directions, their Fourier transforms are cross-shaped. The arms of the crosses have the same orientations in the transforms from corresponding volumes of collagen bundles and filopodia-like structures. The average rotational shift between the transforms from the two sets of volumes is 0.04 ± 0.1 (SD) degrees ($n = 16$), indicating that their orientations in real space are effectively the same (Fig. 3; Movie S10 and Movie S11).

Higher resolution 3D reconstructions on day 12 cornea showed that cell morphology is adaptive toward the orthogonal arrangement of locally secreted collagen; cells showed morphology corresponding to associations with collagen bundles in multiple orientations (Fig. 4). This observation was confirmed in a 3D reconstruction prepared using the IMOD software (36) on SBF SEM images obtained from a volume of dimensions 56 μm × 56 μm × 840 μm (*x*–*y*–*z*, respectively, with the *z* axis at 90° to the corneal surface). Fig. 5 shows two cells (one colored gold, one green) that cross four lamellae (colored white and purple) of total thickness 15 μm. *En face* the cells are aligned with the orthogonal axes of the stroma, with cell processes often seen alongside bundles of collagen fibrils.

Further analyses using EM3D software on image series from the SBF SEM 12-d dataset showed that keratocyte processes appeared closely applied to collagen fibril bundles (Fig. 6 *A* and *B*), exhibiting matched orthogonality when viewed in separate 3D reconstructions (Fig. 6 *C* and *D*). The complexity of interactions between keratocyte processes and collagen fibril bundles was evident in SBF SEM images taken at a section plane perpendicular to the corneal surface (Fig. 7). Observation of component structures in a 3D reconstruction including multiple cell processes and collagen bundles showed that some cell processes adhered closely to individual collagen bundles along the full extent of collagen contained in the reconstructed volume (Fig. 7*A*). In contrast, other processes showed associations with multiple collagen bundles (Fig. 7 *B* and *C*).

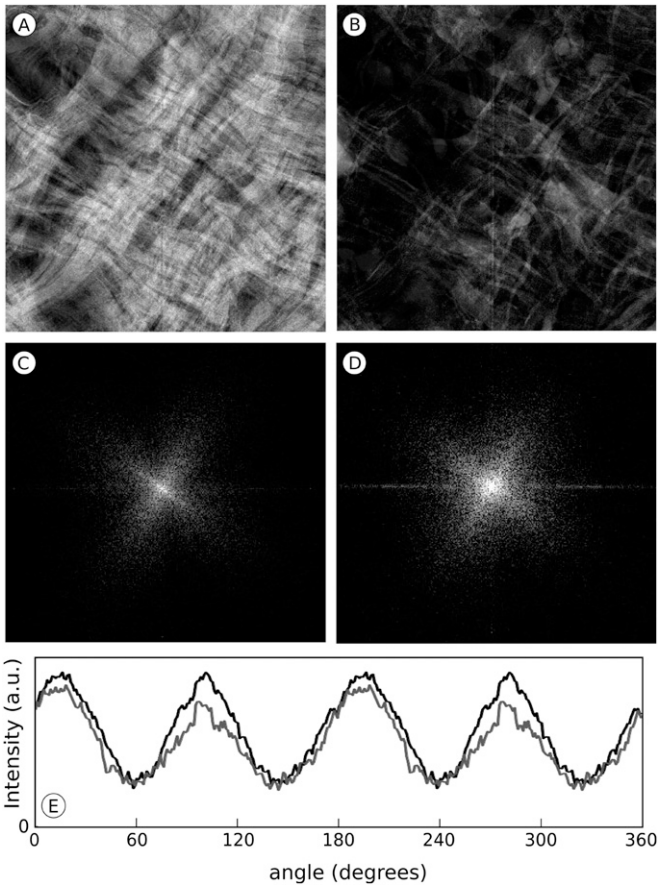

Fig. 3. Analysis of collagen bundle and cellular filopodia directionality in the cornea of a 12-d chicken embryo. A representative volume measuring ~$4.74 \times 4.84 \times 0.33$ μm^3, obtained by SBF SEM in which either the collagen bundles or the filopodia are displayed, is projected down its *z* axis (perpendicular to the corneal surface). (*A*) 2D projection of the volume showing collagen. (*B*) As *A* but of the volume showing filopodia; in *A* and *B* protein density is represented in lighter tones. (*C*) Fourier transform of *A*. (*D*) Fourier transform of *B*. (*E*) Sum of the radial integrated profiles of the transforms from the projections of the collagen bundles (gray) and the filopodia (black) from 16 randomly selected volumes. Peaks arise from the cross-shaped patterns in the transforms; they are ~90° apart and occupy the same positions in both graphs indicating that collagen fibrils and filopodia run parallel to each other, both sets along two mutually orthogonal directions.

Discussion

Here, we present data that permit 3D aspects of corneal matrix formation to be appreciated over tissue volumes larger than previously possible. The data reveal that the proportional volume occupied by cells in relation to extracellular components is unexpectedly high at around 20%. The additional volume contributed by the extensive network of cellular processes, which have been documented previously (28), may not have been fully appreciated in previous studies using 2D imaging techniques. Cell volume is consistently high from day 10 through to day 18 of development. This is somewhat surprising, bearing in mind that stromal keratocytes have rounded morphology at day 10, when a large proportion of the extracellular space is occupied by hyaluronate-rich fluid (37).

Presumptive keratocytes, which early in corneal embryogenesis invade the primary stroma (38), are key to the formation of a mature and functional cornea. The fate of the loose orthogonally arranged collagen bundles of the primary stroma remains poorly understood. By day 10, the first time point examined in our study, the growing stroma has increased in thickness to around 150 microns. It is cellularized at all levels except for the distal 1 μm (4) and is predominantly composed of newly synthesized secondary stromal collagen. Our data do not enable discrimination between secondary and residual primary stroma. It has never been conclusively shown whether the primary stroma acts as a direct template for the orientated deposition of collagen of the secondary stroma, or if this follows from initial positional cues it provides for the invading mesenchymal cells. As the primary

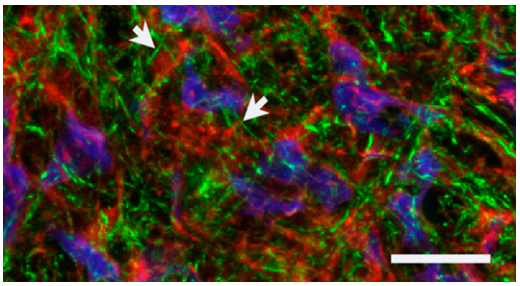

Fig. 2. Chick cornea at 14 d development viewed with 60× oil immersion objective by laser confocal scanning microscopy after immunostaining with antibody for α-actin. Cell nuclei were stained blue with DAPI, and cell membranes and cytoplasm were stained red with Vybrant DiI; actin was stained green with Phalloidin/AlexaFluor 488. Orthogonal cell processes exhibit strong staining for actin (arrows). (Scale bar, 10 μm.)

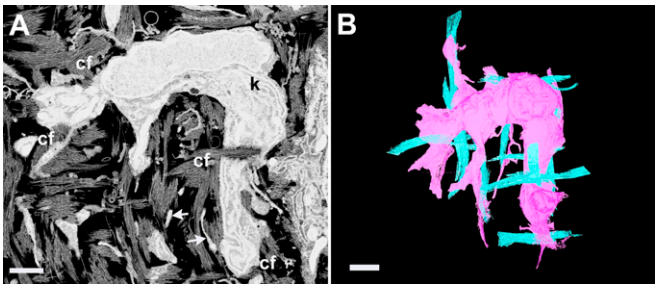

Fig. 4. (*A*) A raw backscatter electron image from an *en face* section of day 12 chick corneal stroma shows a keratocyte (k) with bundles of collagen fibrils (*cf*) closely associated with the cell surface. Keratocyte processes permeate the extracellular space (arrows). (Scale bar, 1 μm.) (*B*) A surface rendering of a 3D reconstruction in EM3D from 100 serial images of the same cell shows orthoganality of cell morphology and associated collagen fibril bundles. (Scale bar, 1 μm.)

stroma becomes dispersed by tissue swelling, cell influx, and new matrix production, subsequent directional signals likely derive from interactions within the keratocyte population.

The 3D reconstructions at day 12 show close association of collagen fibril bundles with the surfaces of keratocytes. Bundles are often enveloped within deep involutions of the cell. The association of cells with multiple bundles displaying quite different fibril orientations invites speculation that individual cells may simultaneously engage in the formation of multiple lamellae. With increased collagen deposition, the cells become more flattened; from embryonic days 12–14 extending long slender processes into the growing stroma Keratocyte processes are reminiscent of filopodia, previously described in migrating cells in healing and developing tissues. It has been suggested that they may function as antennae through which cells detect signals from the extracellular environment. In an early study of embryonic chick corneal fibroblasts, using freeze fracture to reveal details of the cell membranes, these cytoplasmic extensions were referred to as filopodia (39). However, the entire structure could not be revealed in one freeze-fracture plane, and consequently their abundance and considerable length were unappreciated. Filopodia, aligned with secreted collagen fibrils, were also a feature of bovine corneal cells cultured in vitro (40). The 3D reconstructions from our study show that in developing cornea these tubular membrane extensions travel more than 30 microns from the main body of the cell. In the light of recent interest in the structure, assembly, and function of filopodia, particularly as models of protein cascades involved in actin polymerization and depolymerization, it now seems less likely that the cellular extensions from embryonic corneal cells can be regarded as true filopodia. In fact, filopodia in living cells have been described as "dynamic, actin-rich, cylindrical membrane protrusions that extend and retract rapidly" (41). Goh et al. make a compelling case for defining filopodia based upon their characteristic movement in vivo and relatively brief lifetime as much as upon their structure. Volume electron microscopy requires that tissue samples are fixed and resin-embedded, and further investigations imaging living systems are required to clarify the longevity of these structures in embryonic cornea. On a structural basis, filopodia-like structures formed by embryonic corneal cells are actin-rich, and of similar diameter, but exceed greatly in length previous descriptions of filopodia. We suspect that they are also more long-lived than true filopodia, which, for example in living neuronal cells, had a lifetime of only up to 3.5 min (41). Associations between the keratocyte cytoskeleton and collagen trafficking were previously shown following immunolocalization of actin and type I collagen propeptides in embryonic cornea (42). We believe that embryonic corneal filopodia may represent cellular structures with unique dimensions and cornea-specific function, which have a crucial role in orientation and organization of collagen into lamellae, and suggest the term "keratopodia" for these structures.

Keratopodia permit a system of cell–matrix associations to be maintained at sites distant from the main secretory machinery of the cell during the period when collagen bundles increase and grow to fill the fluid extracellular space. It is possible that similarly elongate cellular processes are a feature of other developing tissues that form highly organized matrices, although none have yet been described. In cornea, cell–cell and cell–matrix interactions achieved in this way could conceivably prove advantageous where the function of transparency in the mature tissue requires that the matrix be supported by a small population of cells. It is through these connections, we speculate, that the cell is able to determine the directionality of growing fibril bundles and thus eventually entire lamellae. These remote connections, which the cell maintains with collagen in the expanding matrix, may also facilitate stromal condensation. Feedback to the cell would provide cues for retraction of keratopodia to exert force on deposited collagen, thus bringing about condensation of the stroma that occurs between days 14 and 18 of development.

The 3D reconstructions from SBF SEM show that keratopodia form a striking orthogonal template as early as developmental day 12. Some keratopodia were identified apposed to single collagen bundles, whereas others established contact with multiple bundles. The nature of keratopodial connections with collagen bundles has not yet been fully characterized; preliminary studies show fibronectin and integrin α5 and β1 localization at sites of contact. Retraction of keratopodia by the cell potentially could provide the cell with a mechanism for tensioning bundles of collagen and drawing together individual bundles into the compact lamellar architecture of the mature stroma. The elongated nature of these cell processes effectively provides keratocytes with the potential for long-range interactions with the developing matrix. The 3D views have shown that although some keratopodia terminate alongside collagen bundles, many make

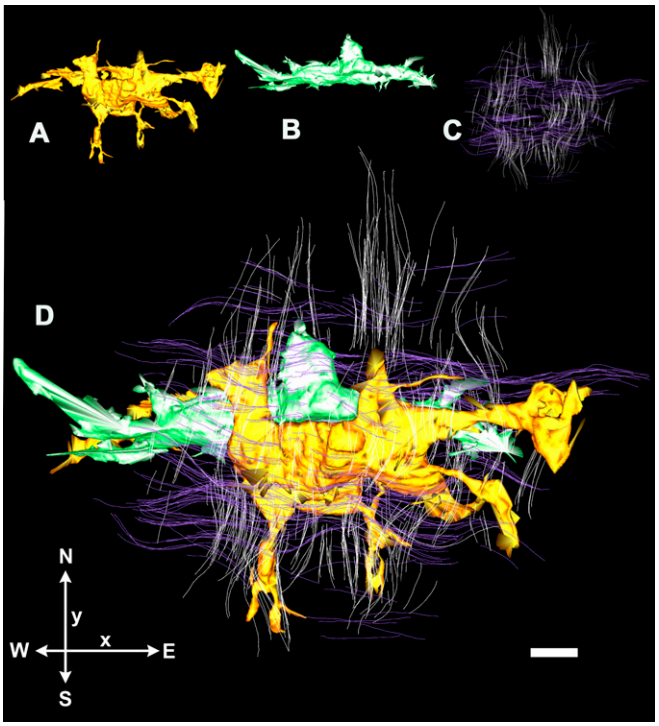

Fig. 5. 3D reconstruction of 1.5 μm × 1.5 μm × 15 μm (*x*–*y*–*z*) volume of day 12 chick corneal stroma in *en face* view, obtained by 3View SBF SEM and IMOD segmentation; *A*–*C* show components of composite image (*D*). (*A* and *B*) Two closely associated cells lie parallel to the *x* axis with processes, parallel to the *y* axis, that interdigitate between orthogonal collagen fibrils (*C*), oriented north–south (white, parallel to *y* axis) and east–west (purple, parallel to *x* axis). (Scale bar, 1 μm.)

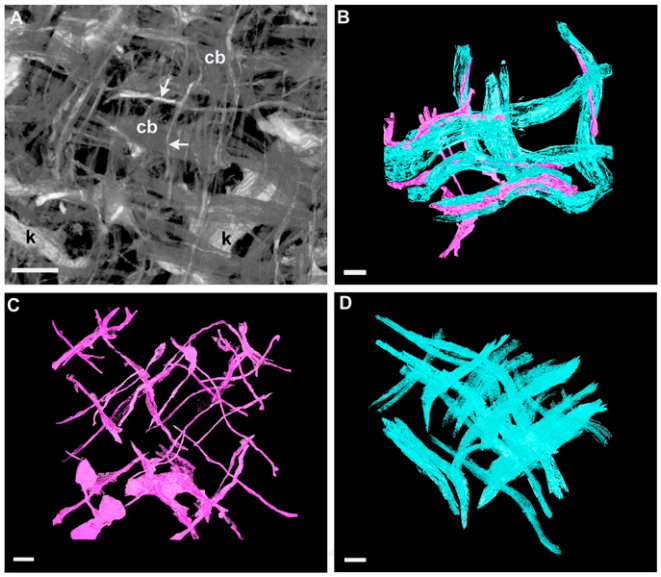

Fig. 6. (*A*) *En face* reconstruction in ImageJ 3D Viewer illustrates orthogonal collagen fibril bundles (cb) and processes (arrows) of keratocytes (k) in day 12 chick cornea. (*B*) Surface rendering in EM3D of a 3D reconstruction of the dataset from *A* reveals close association between keratocyte processes (pink) and collagen fibril bundles (blue). (*C*) The 3D reconstruction in EM3D shows orthogonal orientation of keratocyte processes. (*D*) The 3D reconstruction from same dataset in *C* shows orthogonal collagen fibril bundles. (Scale bars, 500 nm, *A*, and 1 μm, *B*–*D*.)

contact with processes from adjacent cells so that, although not a true syncytium, stromal keratocytes in the embryonic cornea are continuously linked. Intercellular communication throughout the stroma would likely facilitate synchronized activity of keratocytes to coordinate consolidation of fibril bundles into lamellae as development progresses.

Methods

Specimens of Embryonic Cornea. Fertile chicken eggs, obtained from a commercial hatchery (Henry Stewart), were incubated at 37.8 °C and ~58–60% relative humidity, and embryos were removed at embryonic days between 10 and 18. At all times developing embryos were treated in accordance with the Association for Research in Vision and Ophthalmology Statement for the Use of Animals in Ophthalmic and Vision Research and with the approval, under schedule 1, of the UK Government's Animals (Scientific Procedures) Act 1986. Corneas were isolated and fixed by immersion in 2.5% (vol/vol) glutaraldehyde/2% (vol/vol) paraformaldehyde in 0.1 M sodium cacodylate buffer, pH 7.2, for 3 h.

Preparation of Cornea for FIB SEM and SBF SEM. Blocks cut from the corneal center were postfixed for focused ion beam scanning electron microscopy (FIB SEM) for 1 h in 1% (vol/vol) osmium tetroxide containing 1.5% (wt/vol) potassium ferricyanide in 0.1 M sodium cacodylate, followed by 1% (wt/vol) tannic acid for 1 h. Specimens were then infiltrated with 50%, 70%, 90% (all vol/vol) (in water), and 100% Durcupan epoxy resin and embedded and cured at 45 °C for 24 h (32). To enhance the backscatter electron signal to improve imaging of collagen fibrils for serial block face (SBF) SEM, a method developed by Starborg et al. (43) was used. After osmium/ferricyanide as above, specimens were immersed in tannic acid for 2 h, followed by 1% (vol/vol) osmium tetroxide, then 1% (wt/vol) aqueous uranyl acetate for 1 h, each with appropriate washes. These samples were embedded after ethanol dehydration in Araldite CY212 resin.

Transmission Electron Microscopy. Semithin (~3–4 μm) sections of both FIB SEM and SBF SEM blocks were stained with toluidine blue and viewed with a Leica DMRA2 light microscope for orientation and selection of sites for SEM imaging. Matrix ultrastructure was observed in unstained ultrathin sections (~100 nm), collected on copper G300 grids, and examined in a transmission electron microscope (JEM1010, Jeol) operating at 80 kv. Images were acquired with an 11-megapixel 14-bit CCD camera (Orius SC1000; Gatan).

SEM. ***FIB SEM.*** Blocks were mounted on stubs, carbon-coated, and transferred to a Quanta 3D field emission gun (FEG) FIB SEM dual beam scanning electron microscope (FEI Company). After preparation of the imaging surface with a gallium ion beam, the automated software (Slice and View, FEI) was used to acquire a 640 image sequence with a backscatter electron detector, image capture alternating with ion beam slicing. The 50 nm slices were milled at 30 kV and 5 nA beam current, each slice taking 9 s. Images of the milled block face were captured at 5 kV and 4 nA beam current, using a 1,000 μm aperture and 6,000× magnification, a dwell time of 100 μs, and 1,024 × 884 scan resolution, resulting in a magnification of around 50 nm per pixel. Single image acquisition time was 90 s, and total run times for the datasets were between 18–20 h.

SBF SEM. Polished Araldite blocks were glued to aluminum pins after orientation to present a block face either parallel or perpendicular to the corneal surface, for *en face* or meridional sectioning, respectively. They were sectioned using a Gatan 3View ultramicrotome inside an FEI Quanta FEG 250 scanning electron microscope. Sequential backscatter electron images were collected at 4 kv, with a dwell time of 10 μs, alternating with microtome cuts at 100 nm. A scan resolution of 4,096 × 4,096 was selected, equating to 10 nm per pixel.

3D Reconstruction. FIB SEM image stacks from embryonic corneas at 10, 14, and 18 d of development were processed with ImageJ/Fiji software (44) [Summer 2010, http://pacific.mpi-cbg.de/wiki/index.php/Fiji, after Bushby et al. (32)]. Good differential contrast between three component features enabled discrimination between keratocytes, collagen, and intervening fluid spaces. An image area was selected in each dataset corresponding to 38.65 μm and 13.55 μm, respectively, in *x* and *y*. In *z*, the maximum number of artifact-free images in sequence varied in each dataset from 464 from 10 d cornea, through 231 from 14 d cornea, to 570 from 18 d cornea, representing 23, 11, and 28 μm, respectively. Image stacks from each dataset were displayed in 3D Viewer in ImageJ/Fiji. 3View SBF SEM series of up to 1,000 images were acquired from 12 d embryonic cornea sectioned in *en face* or meridional planes. Selected sequences were analyzed using 3D Viewer, or by manual segmentation and 3D rendering using EM3D software (45). Some sequences from *en face* data were used for 3D reconstructions in IMOD (36) as described previously (43).

Fourier Analysis of Keratopodia and Collagen Orthogonality. All image analyses used ImageJ and Fiji image processing software. Sixteen randomly selected volumes measuring ~3.0 × 3.0 × 0.3 μm^3 were selected from a 3View dataset from day 12 embryonic chick cornea. Collagenous and cellular components were distinguishable visually and from their greyscale intensity in the images. By selecting only those gray levels corresponding to collagenous or cellular material, two further sets of volumes were created. The electron density corresponding to the cell bodies was removed manually from the volumes containing the cellular material. The electron density in the two sets of volumes was then projected down their *z* axis (perpendicular to the surface of the cornea) to be analyzed in Fourier space.

A set of straight, randomly spaced, parallel filiform objects in a 2D Real space image is transformed in Fourier space as a straight line, running

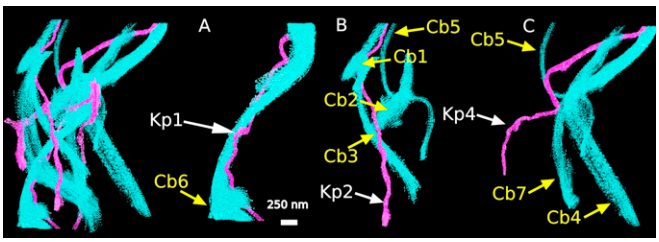

Fig. 7. Surface rendering of a 3D reconstruction from day 12 chick cornea in meridional section reveals associations of collagen bundles (Cb) with individual keratocyte processes (Kp). (*A*–*C*) Structures isolated from the composite reconstruction (far left) demonstrate that some processes associate with only one collagen bundle (*A*, Kp 1 with Cb 6); others have multiple associations (*B*, Kp 2 with Cb 1, 2, 3, and 5; *C*, Kp 4 with Cb 4, 5, and 7). (Scale bar, 250 nm.)

through the origin, at 90° to the direction of the objects in Real space. If the filiform objects in Real space are not perfectly parallel or they are not perfectly straight, the line in Fourier space fans out, with its spread being related to the degree of imperfection of the set of objects in Real space. If there are two sets of filiform objects in Real space that are perpendicular to each other, they are mapped in Fourier space as two straight lines, perpendicular to each other (and also to the original sets of filiform objects in Real space). In the event where two sets of nearly parallel filiform objects are mutually perpendicular in the projections, we expect from theory two sets of perpendicular lines fanning out from the origin of Fourier space. These lines would appear as peaks, 90° apart, in the radial integrals of an annular region around the origin of Fourier space. To analyze the direction of collagen bundles and filopodia, projections from the two sets of volumes were fast Fourier transformed. A circular annulus around the origin, ranging between 1/250 nm^{-1} and 1/50 nm^{-1} and spanning 360°, was selected from each transform and a radial integration performed in this region. The profiles obtained from the transforms of the keratopodia were then aligned by calculating their cross-correlation and summed together. The same was done for the profiles obtained from the collagen bundles, but they were aligned by shifting them by the amounts calculated with the keratopodia profiles. The relative shift between the profiles from the keratopodia and the collagen bundles were also calculated for each of the 16 volumes.

Confocal Immunofluorescence Microscopy Localization of Actin. To relate matrix deposition to cell alignment, the distribution of actin in the cytoskeleton was detected by immunolocalization. Some corneas were snap-frozen unfixed and sectioned at 20 μm on a cryostat. Sections on Histobond glass slides were fixed in 1% paraformaldehyde, washed in PBS, and then incubated with the membrane/cytoplasmic stain Vybrant DiI (20 μM; Invitrogen-Molecular Probes) and actin label Phalloidin/AlexaFluor 488 conjugate (10 μg/mL) in PBS for 24 h at 4 °C. Sections were mounted in Vectorshield with DAPI for nuclear context and viewed with a 60× oil immersion objective on a Leica SP2 AOBS confocal laser scanning microscope, imaging red/green/blue channels simultaneously.

ACKNOWLEDGMENTS. This study was supported by project grants from the Biotechnology and Biological Sciences Resource Council (BB/f022077/1 to C.K. and A.J.Q.) and Engineering and Physical Sciences Research Council (EPSRC; EP/F034970 to A.J.Q. and R.D.Y.) and a programme grant from the Medical Research Council (MR/K000837/1). Use of the FEI Quanta 3D microscope at Queen Mary University of London was funded by an EPSRC Access to Equipment Scheme Grant EP/F019882/1, to A.J.B.). Data from SBF SEM were obtained on the FEI Quanta 250 FEG SEM with Gatan 3View at the Wellcome Trust Centre for Cell-Matrix Research, University of Manchester, funded by Wellcome Trust Grants 091840/Z/10/Z, 083898/Z/07/Z, and 081406/Z/06/Z (to K.E.K.).

1. Ricard-Blum S (2011) The collagen family. *Cold Spring Harb Perspect Biol* 3(1):a004978.
2. Gelse K, Pöschl E, Aigner T (2003) Collagens—Structure, function, and biosynthesis. *Adv Drug Deliv Rev* 55(12):1531–1546.
3. Boote C, Dennis S, Huang Y, Quantock AJ, Meek KM (2005) Lamellar orientation in human cornea in relation to mechanical properties. *J Struct Biol* 149(1):1–6.
4. Trelstad RL, Coulombre AJ (1971) Morphogenesis of the collagenous stroma in the chick cornea. *J Cell Biol* 50(3):840–858.
5. Ruggeri A, Benazzo F, Reale E (1979) Collagen fibrils with straight and helicoidal microfibrils: A freeze-fracture and thin-section study. *J Ultrastruct Res* 68(1):101–108.
6. Holmes DF, et al. (2001) Corneal collagen fibril structure in three dimensions: Structural insights into fibril assembly, mechanical properties, and tissue organization. *Proc Natl Acad Sci USA* 98(13):7307–7312.
7. Raspanti M, Reguzzoni M, Protasoni M, Martini D (2011) Evidence of a discrete axial structure in unimodal collagen fibrils. *Biomacromolecules* 12(12):4344–4347.
8. Kadler KE, Holmes DF, Trotter JA, Chapman JA (1996) Collagen fibril formation. *Biochem J* 316(Pt 1):1–11.
9. Holmes DF, Kadler KE (2005) The precision of lateral size control in the assembly of corneal collagen fibrils. *J Mol Biol* 345(4):773–784.
10. Birk DE, Fitch JM, Babiarz JP, Linsenmayer TF (1988) Collagen type I and type V are present in the same fibril in the avian corneal stroma. *J Cell Biol* 106(3):999–1008.
11. Linsenmayer TF, et al. (1993) Type V collagen: Molecular structure and fibrillar organization of the chicken α 1(V) NH_2-terminal domain, a putative regulator of corneal fibrillogenesis. *J Cell Biol* 121(5):1181–1189.
12. Birk DE, Fitch JM, Babiarz JP, Doane KJ, Linsenmayer TF (1990) Collagen fibrillogenesis in vitro: Interaction of types I and V collagen regulates fibril diameter. *J Cell Sci* 95(Pt 4): 649–657.
13. Birk DE (2001) Type V collagen: Heterotypic type I/V collagen interactions in the regulation of fibril assembly. *Micron* 32(3):223–237.
14. Segev F, et al. (2006) Structural abnormalities of the cornea and lid resulting from collagen V mutations. *Invest Ophthalmol Vis Sci* 47(2):565–573.
15. Birk DE, Trelstad RL (1986) Extracellular compartments in tendon morphogenesis: Collagen fibril, bundle, and macroaggregate formation. *J Cell Biol* 103(1):231–240.
16. Birk DE, Zycband E (1994) Assembly of the tendon extracellular matrix during development. *J Anat* 184(Pt 3):457–463.
17. Birk DE, Zycband EI, Woodruff S, Winkelmann DA, Trelstad RL (1997) Collagen fibrillogenesis in situ: Fibril segments become long fibrils as the developing tendon matures. *Dev Dyn* 208(3):291–298.
18. Zhang G, et al. (2005) Development of tendon structure and function: Regulation of collagen fibrillogenesis. *J Musculoskelet Neuronal Interact* 5(1):5–21.
19. Canty EG, et al. (2004) Coalignment of plasma membrane channels and protrusions (fibripositors) specifies the parallelism of tendon. *J Cell Biol* 165(4):553–563.
20. Humphries SM, Lu Y, Canty EG, Kadler KE (2008) Active negative control of collagen fibrillogenesis *in vivo*. Intracellular cleavage of the type I procollagen propeptides in tendon fibroblasts without intracellular fibrils. *J Biol Chem* 283(18):12129–12135.
21. Starborg T, Lu Y, Huffman A, Holmes DF, Kadler KE (2009) Electron microscope 3D reconstruction of branched collagen fibrils in vivo. *Scand J Med Sci Sports* 19(4): 547–552.
22. Giraud-Guille MM (1996) Twisted liquid crystalline supramolecular arrangements in morphogenesis. *Int Rev Cytol* 166:59–101.
23. Giraud-Guille MM, Besseau L, Martin R (2003) Liquid crystalline assemblies of collagen in bone and in vitro systems. *J Biomech* 36(10):1571–1579.
24. Guo X, et al. (2007) Morphologic characterization of organized extracellular matrix deposition by ascorbic acid-stimulated human corneal fibroblasts. *Invest Ophthalmol Vis Sci* 48(9):4050–4060.
25. Saeidi N, et al. (2012) Molecular crowding of collagen: A pathway to produce highly-organized collagenous structures. *Biomaterials* 33(30):7366–7374.
26. Hay ED (1980) Development of the vertebrate cornea. *Int Rev Cytol* 63:263–322.
27. Hay ED, Revel JP (1969) *Fine Structure of the Developing Avian Cornea. Monographs in Developmental Biology* (S Karger, New York).
28. Birk DE, Trelstad RL (1984) Extracellular compartments in matrix morphogenesis: Collagen fibril, bundle, and lamellar formation by corneal fibroblasts. *J Cell Biol* 99(6):2024–2033.
29. Hekking LHP, et al. (2009) Focused ion beam-scanning electron microscope: Exploring large volumes of atherosclerotic tissue. *J Microsc* 235(3):336–347.
30. Knott G, Marchman H, Wall D, Lich B (2008) Serial section scanning electron microscopy of adult brain tissue using focused ion beam milling. *J Neurosci* 28(12):2959–2964.
31. Armer HEJ, et al. (2009) Imaging transient blood vessel fusion events in zebrafish by correlative volume electron microscopy. *PLoS ONE* 4(11):e7716.
32. Bushby AJ, et al. (2011) Imaging three-dimensional tissue architectures by focused ion beam scanning electron microscopy. *Nat Protoc* 6(6):845–858.
33. Heymann JA, et al. (2006) Site-specific 3D imaging of cells and tissues with a dual beam microscope. *J Struct Biol* 155(1):63–73.
34. Leighton SB (1981) SEM images of block faces, cut by a miniature microtome within the SEM—A technical note. *Scan Electron Microsc* 233(Pt 2):73–76.
35. Denk W, Horstmann H (2004) Serial block-face scanning electron microscopy to reconstruct three-dimensional tissue nanostructure. *PLoS Biol* 2(11):e329.
36. Kremer JR, Mastronarde DN, McIntosh JR (1996) Computer visualization of three-dimensional image data using IMOD. *J Struct Biol* 116(1):71–76.
37. Toole BP, Trelstad RL (1971) Hyaluronate production and removal during corneal development in the chick. *Dev Biol* 26(1):28–35.
38. Quantock AJ, Young RD (2008) Development of the corneal stroma, and the collagen-proteoglycan associations that help define its structure and function. *Dev Dyn* 237(10): 2607–2621.
39. Hasty DL, Hay ED (1977) Freeze-fracture studies of the developing cell surface. I. The plasmalemma of the corneal fibroblast. *J Cell Biol* 72(3):667–686.
40. Bueno EM, Saeidi N, Melotti S, Ruberti JW (2009) Effect of serum and insulin modulation on the organization and morphology of matrix synthesized by bovine corneal stromal cells. *Tissue Eng Part A* 15(11):3559–3573.
41. Goh WI, et al. (2011) Rif-mDia1 interaction is involved in filopodium formation independent of Cdc42 and Rac effectors. *J Biol Chem* 286(15):13681–13694.
42. Gealy C, et al. (2009) Actin and type I collagen propeptide distribution in the developing chick cornea. *Invest Ophthalmol Vis Sci* 50(4):1653–1658.
43. Starborg T, et al. (2013) Using transmission electron microscopy and 3View to determine collagen fibril size and three-dimensional organization. *Nat Protoc* 8(7): 1433–1448.
44. Abramoff MD, Magelhaes PJ, Ram SJ (2004) Image processing with ImageJ. *Biophotonics International* 11(7):36–42.
45. Ress DB, Harlow ML, Marshall RM, McMahan UJ (2004) Methods for generating high-resolution structural models from electron microscope tomography data. *Structure* 12(10):1763–1774.